8

PROSPECTS FOR COMPUTING AIRFOIL AERODYNAMICS WITH REYNOLDS AVERAGED NAVIER-STOKES CODES

George S. Deiwert and H. E. Bailey
NASA Ames Research Center

SUMMARY

The Reynolds averaged Navier-Stokes equations are solved numerically for a variety of transonic airfoil configurations where viscous phenomena are important. Illustrative examples include flows past sensitive geometries, Reynolds number effects, and buffet phenomena.

INTRODUCTION

The prediction of viscous phenomena in airfoil aerodynamics involves descriptions of both boundary-layer and inviscid flow regions and their interaction with one another. For flows where the boundary layer remains attached, the two flow regions may be analyzed separately and their interaction determined iteratively. This generally requires solving the compressible Euler equations (or a suitable subset) for the inviscid field and the boundary-layer equations for the viscous region near solid surfaces. The flow regions posing computational difficulty in these cases are the near wake, with its trailing edge singularity, and possible shock/boundary-layer interaction regions. When the viscous-inviscid interactions are strong, and there is flow separation or even buffeting, it is more reasonable to solve the Navier-Stokes equations for compressible flows. These equations describe the coupling between the viscous and inviscid regions, describe the elliptic behavior in regions of flow separation, and do not contain the singularity at the trailing edge.

In this paper several illustrative examples are presented in which viscous effects are important to transonic airfoil flows. All viscous numerical solutions are obtained from the Reynolds averaged Navier-Stokes equations and all are compared with appropriate experimental data. Two computer codes are used at present to generate flow field solutions: a fully implicit code, described in reference 1, and a mixed explicit/implicit code, described in reference 2. Both produce comparable results and are competitive in their computational efficiency. Symbol definitions are given in an appendix.

SHOCKLESS LIFTING AIRFOIL

Consider first the shock-free supercritical profile designed analytically by Garabedian and Korn (ref. 3). A series of experiments for design and

off-design conditions were performed at the NAE by Kacprzynski et al. (ref. 4) and by Kacprzynski (ref. 5). Comparisons at the design conditions with the inviscid theory of Garabedian and Korn suggest that the wind-tunnel test conditions for Mach number and angle of attack be corrected by subtracting 0.015 and 0.89°, respectively. This was in fact done and a series of comparisons between experiment and inviscid theory were made at a variety of off-design conditions (ref. 4). Figure 1 shows one such comparison for a test Mach number of 0.755 and an angle of attack of 0.12°, just slightly off the design conditions of 0.750 and 0.0°, respectively. Included are inviscid solutions for both the corrected ($M = 0.740$, $\alpha = -0.77°$) and uncorrected conditions. Clearly, the "corrected" solution shows better agreement with experiment, though it fails to predict drag coefficient C_D accurately. Also included in this figure is a viscous solution from a Navier-Stokes code at the uncorrected test conditions. The inclusion of viscous effects results in the same overall improvement as correcting the wind tunnel test conditions. Furthermore, both drag and lift are predicted accurately.

A second example, shown in figure 2, is for a high-lift configuration, where the test Mach number is 0.747 and angle of incidence is 2.96°. As in figure 1, the corrected inviscid solution for $M = 0.732$ and $\alpha = 2.07°$ agrees much better with experiment than do the uncorrected inviscid results. Again, drag is not well predicted and, in this case, neither is lift. Inclusion of viscous effects, by means of the Navier-Stokes equations, results in similar overall improvement without corrections to wind tunnel test conditions. However, both drag and lift are better predicted.

Kacprzynski et al. (ref. 4) state that the only justification for their correction is that it leads to the best agreement in pressure distribution between theory and experiment for the design case. In addition, the large discrepancies, particularly in Mach number, were not explainable. Previous experience indicated that Mach number corrections should be practically zero and angle of attack corrections less than 0.89°. It is suggested here, based on the results shown in figures 1 and 2, that viscous effects are of primary consideration for this particular airfoil configuration, and that tunnel corrections, while probably necessary, are not as great as indicated by inviscid theory.

Two possible explanations for this sensitivity of an inviscid design to viscous effects are: 1) the critical rapid expansion region at the nose of the airfoil is altered by viscous effects, and 2) the high aft camber results in fairly large viscous displacement thicknesses. Hence, we find an inviscid design producing a configuration that is highly sensitive to viscous phenomena.

To further support the validity of viscous solutions, a series of computations were made for nominal test Mach numbers of 0.75 and angles of attack ranging from -1.54° to 4.34°. The results of these computations are compared with experiment in figure 3 in the form of a drag polar (fig. 3(a)) and lift curve (fig. 3(b)). The agreement in both cases is very good.

Included in the drag polar are linearized inviscid results (which, of course, predict zero drag) and nonlinear inviscid results from the Garabedian and Korn code. The viscous solutions for angles of incidence greater than 3°

indicate buffet and are illustrated by two C_L vs C_D branches for angles 3.25° and 4.34°. The lift and drag vary periodically along the branch corresponding to the particular angle of incidence. Other angles of incidence greater than 3° (not shown) would exhibit different paths of periodic variation.

The buffet domain is more clearly illustrated in figure 3(b) for lift as a function of angle of attack. Here, for a given incidence, the minimum and maximum lift values define a buffet envelope. Note that the buffet onset and buffet boundaries are not necessarily confirmed nor repudiated by experiment. The experiments were static and not designed to define buffet conditions. The correspondence of maximum C_L, however, suggests similar buffet onset in the experiment.

To realize agreement between computation and experiment, the results shown in the lift curve suggest, for no Mach number corrections, suitable angle of attack corrections of roughly -0.3° for the 6% wall porosity experiment of reference 4 and -1.3° for the 20.5% wall porosity experiment of reference 5.

NACA 0012 AIRFOIL

Recent experiments in the AEDC 1-ft transonic tunnel on an NACA 0012 airfoil by Kraft and Parker were compared with similar experiments by Vidal et al. (ref. 6) in the Calspan 8-ft transonic tunnel. Results for a test Mach number of 0 80 and a 1° angle of attack indicate differences in shock position and trailing edge pressure between the two experiments. Two possible explanations for these discrepancies included 1) differences in wind-tunnel effect and 2) a Reynolds number effect. The Calspan experiments were performed at a chord Reynolds number of 1.0×10^6 and the AEDC experiments at 2.25×10^6. Computed Navier-Stokes solutions for each of these Reynolds numbers were compared with experiment by Potter and Adams (ref. 7) for upper surface pressure distribution and are reproduced in figure 4. The computed results agree with experiment at corresponding Reynolds numbers, suggesting that the difference in shock position is due to a Reynolds number effect. The low Reynolds number solution ($Re = 1\times10^6$) indicates the presence of separated flow downstream of the mid-chord position while the high Reynolds number solution ($Re = 2.25\times10^6$) is attached. This difference in flow pattern is reasonable in view of the fact that the low Reynolds number flow is transitional near the mid-chord of the airfoil and thus more susceptible to separation than the fully developed, higher Reynolds number flow. There are insufficient experimental data to confirm the existence or absence of separated flow.

Included for comparison in figure 4 is an inviscid solution obtained from transonic small perturbation theory (ref. 7). It is seen by comparison that for these relatively low Reynolds numbers the consideration of viscous effects is important since the lift coefficient may be strongly affected by shock wave location, which in turn is strongly affected by viscosity.

CIRCULAR ARC (18%)

A series of experiments and computations for the transonic flow over an 18% biconvex circular arc airfoil has been performed at the Ames Research Center (refs. 8-15). Results from these studies indicate the existence of three separate flow domains that are defined by Mach number and Reynolds number. Figure 5, taken from reference 12, shows the experimentally determined boundaries of these flow domains. For Mach numbers less than 0.73, the flow is always steady, with flow separation occurring near the trailing edge of the airfoil. For Mach numbers greater than 0.78, the flow is always steady, with separation occurring at the foot of the shock and closing in the near wake. In between exists an unsteady periodic regime in which the flow alternates between shock-induced separation and fully attached flow.

Surface pressure comparisons between viscous computations and experiment in each of the three flow regimes is shown in figure 6 (taken from ref. 14). For the low Mach number ($M = 0.72$) steady flow with trailing edge separation, the agreement is excellent. For the high Mach number ($M = 0.783$) steady flow with shock-induced separation, the comparisons are only qualitatively correct. In this case the computed solution indicates the presence of a strong oblique shock, while the experiment indicates a weak oblique shock. While both strong and weak shock solutions will satisfy the governing equations, the computer code at present does not yield the weak solution shown in the experiment. Both computation and experiment exhibit shock-induced separation with closure realized in the near wake. Size of the reverse flow region is reasonably well predicted (see refs. 13 and 15). For the unsteady flow regime, the pressure distribution over the airfoil surface is unsteady. Comparisons for this case will be discussed subsequently.

Shown in figure 7 are selected frames from a high-speed shadowgraph movie of the upper aft portion of the airfoil during experimental tests. Figure 7(a) shows a normal shock at about 65% chord with flow separation occurring just ahead of the trailing edge. This corresponds to the low Mach number regime. Figure 7(b) shows a time-dependent sequence of the same region for the unsteady regime and illustrates the periodic nature of the alternating shock-induced separation/fully attached flow. Figure 7(c) shows a steady oblique shock at nearly 60% chord with separation initiated at the foot of the shock.

Figure 8 shows computed Mach contours for the three flow regimes; figures 8(a), 8(b), and 8(c) correspond to steady flow with trailing edge separation, unsteady periodic flow, and steady flow with shock-induced separation, respectively. The comparison of results between figures 7 and 8 illustrates that the computer simulation reflects the appropriate physical behavior of this configuration and describes all three flow regimes observed experimentally. The only real point of discrepancy remains in the weak vs strong oblique shock in the steady flow high Mach number case.

Finally, in figure 9, the surface pressure time histories for the computed and experimental unsteady flows are compared. Flow conditions were for $M = 0.754$, $\alpha = 0°$, and $Re = 11 \times 10^6$ in both the computation and experiment. The computed results simulated the wind-tunnel walls as boundary conditions.

Comparisons are made at a mid-chord location and near a 3/4-chord location on both upper and lower surfaces simultaneously. Remarkable agreement is found both in form and amplitude of the variations. The reduced frequency of the oscillations agreed to within 20%.

Clearly, viscous effects are important in all three flow regimes observed for the 18% circular arc airfoil. The success of the computer code in simulating such flows, particularly in the unsteady regime, gives confidence in its utility.

COMPUTATIONAL EFFICIENCY

At present, two computer codes are used at Ames to solve the Reynolds averaged Navier-Stokes equations for compressible flows. One is based on the mixed explicit/implicit algorithm developed by MacCormack (ref. 16) and the other on the fully implicit algorithm developed by Beam and Warming (refs. 17 and 18) and Briley and McDonald (ref. 19). Both codes are competitive in terms of cost and reliability of results. In addition, both codes are in a continued state of development and are constantly being improved in terms of efficiency. For example, flow over the Korn airfoil was simulated using the fully explicit code of 1974 and required 13 hr of CDC 7600 time to obtain a converged solution. An improved version (1976) employing a mixed explicit/implicit operator reduced the computer requirements to 90 to 120 min. The present version (mixed explicit/implicit, 1978) requires only 20 to 30 min for the same configuration. Modifications are presently underway to reduce this time by one-half.

Both of the present codes use algebraic eddy viscosity models to describe the Reynolds stresses in terms of mean field gradients. Discussions of these models for the mixed code are presented in references 8, 9, and 13 and for the fully implicit code by Baldwin and Lomax (ref. 20). It is possible that these models can have a significant influence on the reliability of the results. A continued effort exists at Ames to further improve the reliability of the turbulence transport models.

CONCLUDING REMARKS

Three illustrative examples have shown that consideration of viscous effects is important for computing airfoil aerodynamics in a variety of situations. Included are sensitive shapes (such as the Korn supercritical airfoils), the definition of buffet boundaries, Reynolds number effects, separated flows, and unsteady flows. In addition it has been shown, by comparison with experiment, that computer codes based on the Reynolds averaged Navier-Stokes equations can provide adequate simulations of these flows for the evaluation of a given design. The computational efficiency of these codes is steadily being improved such that they are expected to be an effective analytical tool in the near future.

APPENDIX

SYMBOLS

c	airfoil chord
C_D	drag coefficient
C_L	lift coefficient
C_p	pressure coefficient
C_p^*	critical pressure coefficient
M	free-stream Mach number
P_t	total pressure
Re	free-stream Reynolds number based on chord
t	time
x	chordwise coordinate
α	free-stream angle of attack
ΔP	incremental pressure from the mean surface pressure

REFERENCES

1. Steger, J. L.: Implicit Finite Difference Simulation of Flow About Arbitrary Geometries with Application to Airfoils. AIAA Paper 77-665, June 1977.

2. Deiwert, G. S.: Recent Computation of Viscous Effects in Transonic Flow. A. I. van de Vooren and P. J. Zandberge, eds., Lecture Notes in Physics 59, Springer-Verlag, New York, 1976, pp. 159-164.

3. Garabedian, P. R., and Korn, D. G.: Numerical Design of Transonic Airfoils. Numerical Solution of Partial Differential Equations - II. Academic Press, New York, 1971, pp. 253-271.

4. Kacprzynski, J. J.; Ohman, L. H.; Garabedian, P. R.; and Korn, D. G.: Analysis of the Flow Past a Shockless Lifting Airfoil in Design and Off-design Conditions. NRC, Aeronautical Report LR-554, Nov. 1971.

5. Kacprzynski, J. J.: A Second Series of Wind Tunnel Tests of the Shockless Lifting Airfoil No. 1. NRC/NAE Wind Tunnel Project Report 5x5/0062, June 1972.

6. Vidal, R. J.; Catlin, P. A.; and Chudyk, D. W.: Two-Dimensional Subsonic Experiments with an NACA 0012 Airfoil. Calspan Report No. RK-5070-A-3, Dec. 1973.

7. Potter, J. L.; and Adams, J. C.: Computational Aerodynamics Requirements in Conjunction with Experimental Facilities. Future Computer Requirements for Computational Aerodynamics, NASA CP-2032, Feb. 1978.

8. Deiwert, G. S.: Numerical Simulation of High Reynolds Number Transonic Flows. AIAA Journal, vol. 13, Oct. 1975, pp. 1354-1359.

9. Deiwert, G. W.: High Reynolds Number Transonic Flow Simulation. R. D. Richtmyer, ed., Lecture Notes in Physics 35, Springer-Verlag, New York, 1975, pp. 132-137.

10. Deiwert, G. W.; McDevitt, J. B.; and Levy, L. L., Jr.: Simulation of Turbulent Transonic Separated Flow Over an Airfoil. Aerodynamic Analyses Requiring Advanced Computers, Part I, NASA SP-347, 1975.

11. Baldwin, B. S.; MacCormack, R. W.; and Deiwert, G. S.: Numerical Techniques for the Solution of the Compressible Navier-Stokes Equations and Implementation of Turbulence Models. Computational Methods for Inviscid and Viscous Two- and Three-Dimensional Flow Fields, AGARD-LS-73, Feb. 1975.

12. McDevitt, J. B.; Levy, L. L. Jr.; and Deiwert, G. S.: Transonic Flow about a Thick Circular-Arc Airfoil. AIAA Jornal, vol. 14, May 1976, pp. 606-613.

13. Deiwert, G. S.: Computation of Separated Transonic Turbulent Flows. AIAA Journal, vol. 14, June 1976, pp. 735-740.

14. Levy, L. L. Jr.: An Experimental and Computational Investigation of the Steady and Unsteady Transonic Flow Field About an Airfoil in a Solid-Wall Test Channel. AIAA Paper 77-678, June 1977.

15. Seegmiller, H. L.; Marvin, J. G.; and Levy, L. L. Jr.: Steady and Unsteady Transonic Flow. AIAA Paper 78-160, Jan. 1978.

16. MacCormack, R. W.: An Efficient Explicit-Implicit-Characteristic Method for Solving the Compressible Navier-Stokes Equations. SIAM-AMS Proceedings of the Symposium on Computational Fluid Dynamics, New York, April 16-17, 1977.

17. Beam, R.; and Warming, R. F.: An Implicit Finite-Difference Algorithm for Hyperbolic Systems in Conservation-Law-Form. J. Comp. Physics, vol. 22, Sept. 1976, pp. 87-110.

18. Beam, R.; and Warming, R. F.: An Implicit Factored Scheme for the Compressible Navier-Stokes Equations. AIAA Paper 77-645, June 1977.

19. Briley, W. R.; and McDonald, H.: An Implicit Numerical Method for the Multi-Dimensional Compressible Navier-Stokes Equations. Report M911363-6, United Aircraft Research Laboratories, 1973.

20. Baldwin, B. S.; and Lomax, H.: Thin Layer Approximation and Algebraic Model for Separated Turbulent Flows. AIAA Paper 78-257, Jan. 1978.

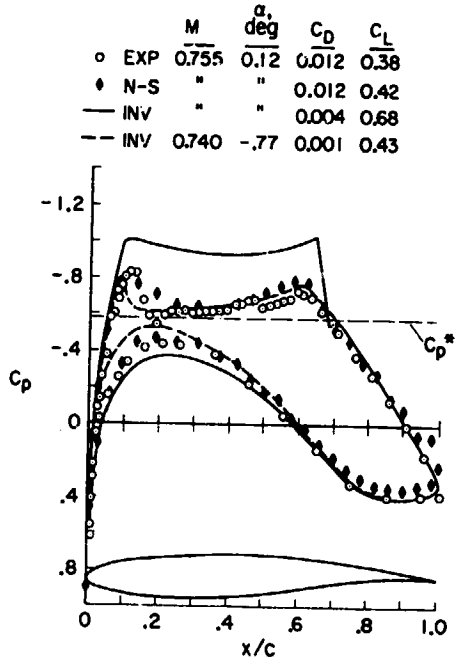

Figure 1.- Surface pressure distribution over Korn 1 airfoil at near-design conditions. Re = 21 × 10^6.

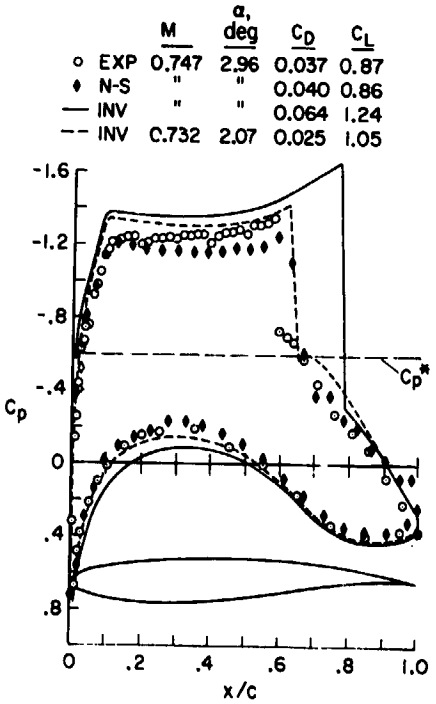

Figure 2.- Surface pressure distribution over Korn 1 airfoil at high lift conditions. Re = 21 × 10^6.

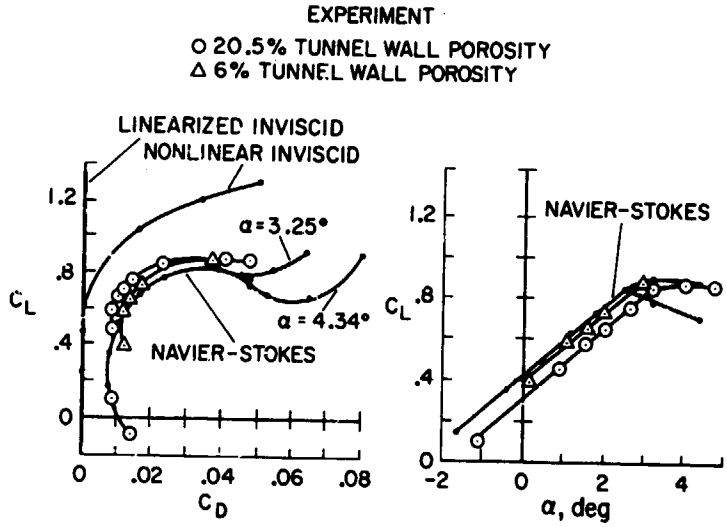

(a) Drag polar. (b) Lift curve.

Figure 3.- Drag polar and lift curve for Korn 1 airfoil at nominal Mach number of 0.75. Re = 21 × 10^6.

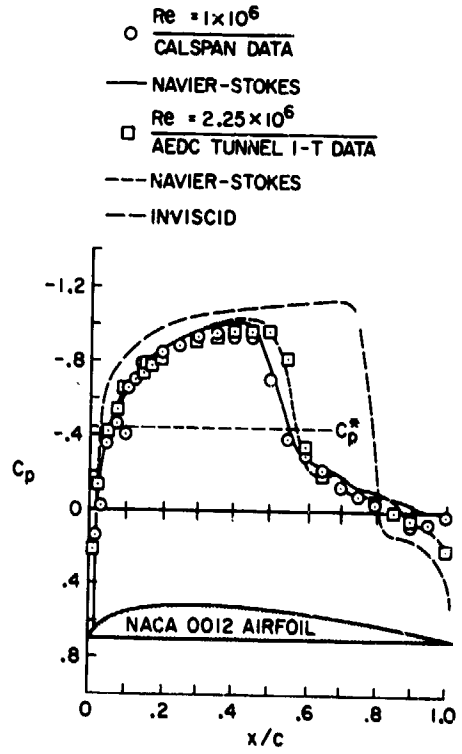

Figure 4.- Upper surface pressure distribution over NACA 0012 airfoil. M = 0.80; α = 1°.

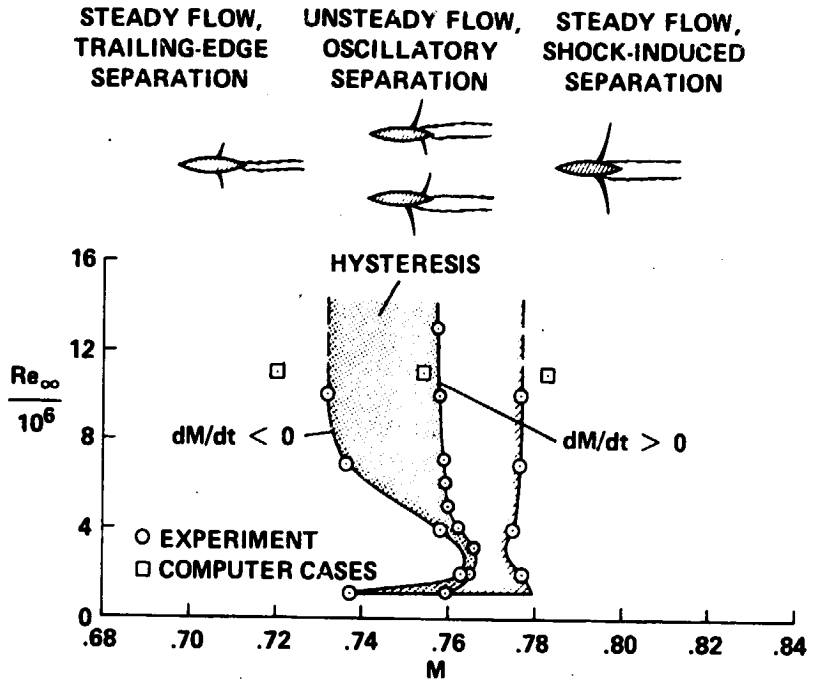

Figure 5.- Experimental flow domains for the 18-percent-thick circular-arc airfoil.

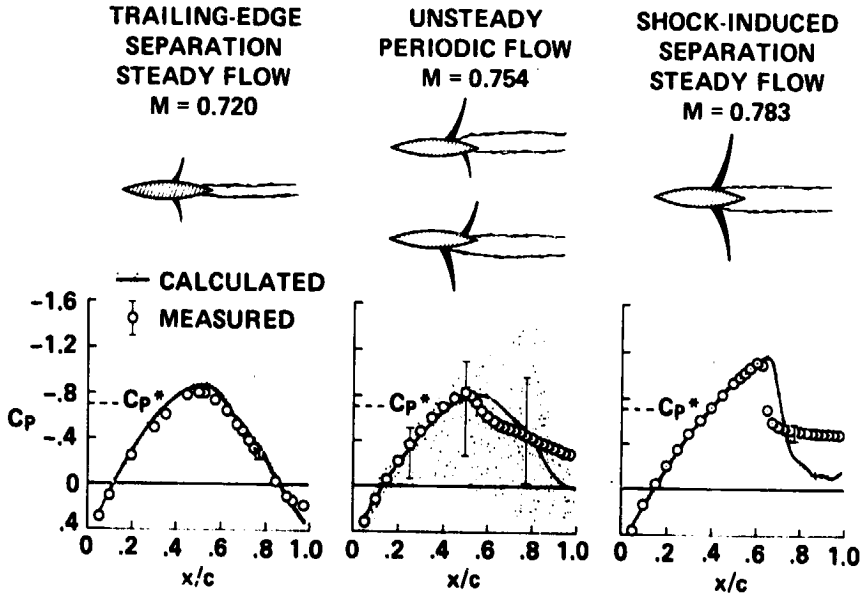

Figure 6.- Computed and experimental pressure distributions on the 18-percent-thick circular-arc airfoil. Re = 11 × 10^6; $\alpha = 0°$.

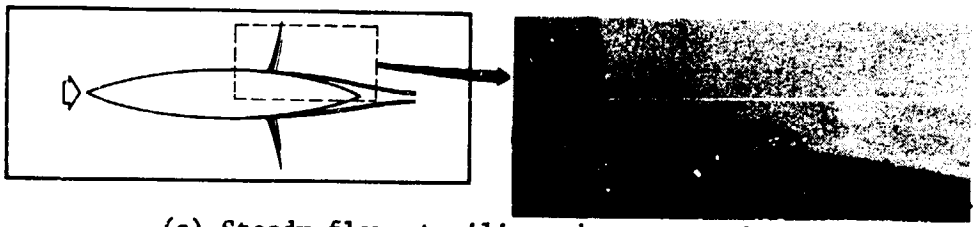

(a) Steady-flow, trailing-edge separation.

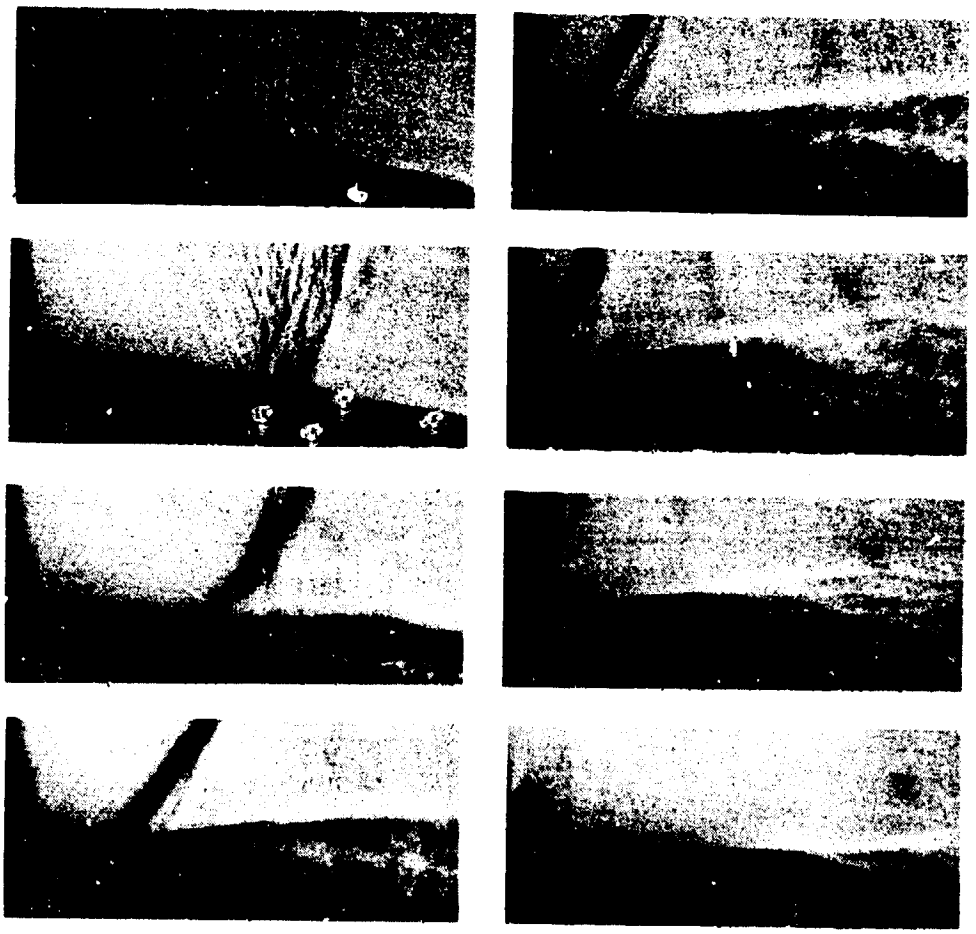

(b) Unsteady flow, oscillatory separation.

(c) Steady flow, shock-induced separation.

Figure 7.- Boundary-layer separation on the 18-percent-thick circular-arc airfoil from a shadowgraph movie. Re = 11 × 10^6; $\alpha = 0^o$.

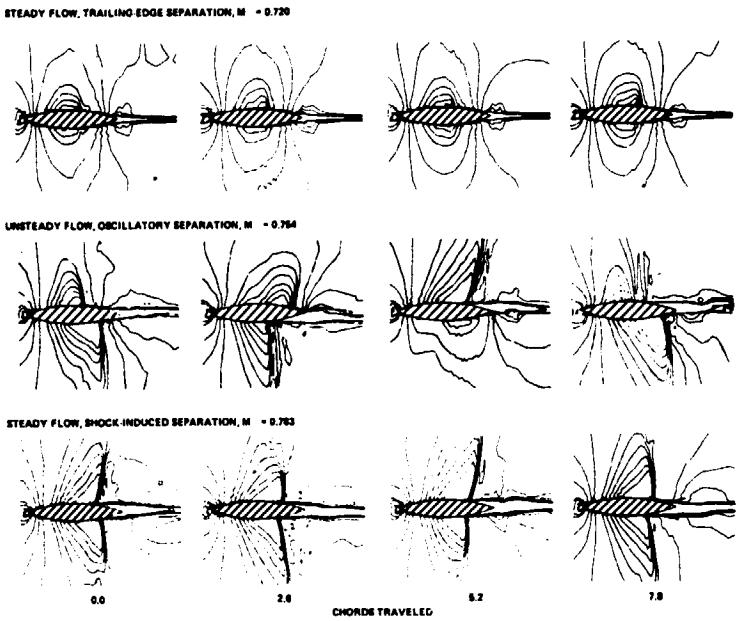

Figure 8.- Computed Mach contours in the flow field about the 18-percent-thick circular-arc airfoil. Re = 11 × 10^6; α = 0°.

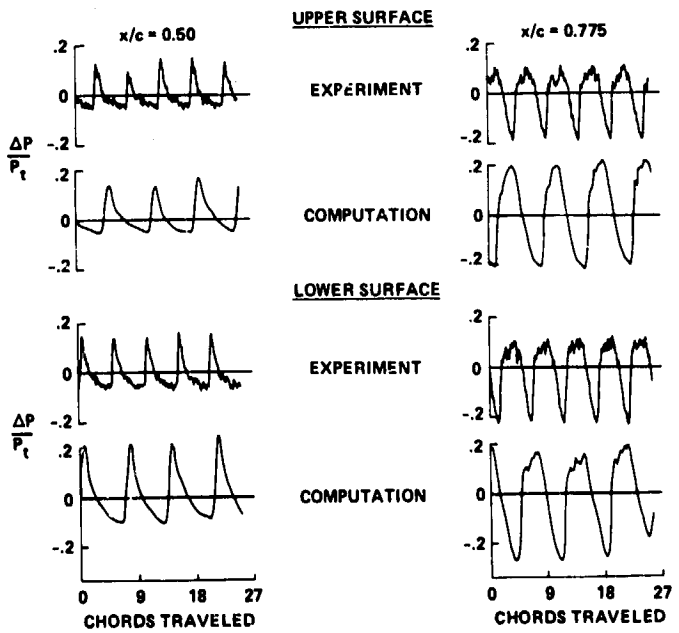

Figure 9.- Surface pressure time histories on the 18-percent-thick circular-arc airfoil with unsteady flow. M = 0.76; Re = 11 × 10^6; α = 0°.